Electrocatalytic activity and volatile product selectivity for nitrate reduction at tin-modified Pt(100), Pd(100) and Pd–Pt(100) single crystal electrodes in acidic media

Masaru Kato,[a,b*] Yuki Unuma,[b] Manabu Okui,[b] Yunteng Qu,[c†] Jinhang Zheng,[b] Satoshi Taguchi,[e] Fumiya Kiguchi,[d] Mashu Torihata,[d] Yunzhi Gao,[c] Nagahiro Hoshi,[d] Ichizo Yagi [a,b*]

[a]Faculty of Environmental Earth Science and [b]Graduate School of Environmental Science, Hokkaido University, N10W5, Kita-ku, Sapporo 060-0810, Japan

[c]School of Chemistry and Chemical Engineering, Harbin Institute of Technology, No. 92 West-Da Zhi Street, Harbin 150001, People's Republic of China

[d]Department of Applied Chemistry and Biotechnology, Graduate School of Engineering, Chiba University, Yayoi-cho 1-33, Inage-ku, Chiba 256-8522, Japan

[e]Laboratory of Chemistry, Hokkaido University of Education Sapporo, Ainosato 5-3-1, Kita-ku, Sapporo 002-8502, Japan

†Present address: State Key Laboratory of Photoelectric Technology and Functional Materials, International Collaborative Center On Photoelectric Technology and Nano Functional Materials, Institute of Photonics and Photon-Technology, Northwest University, Xi'an 710069, People's Republic of China

Corresponding authors

*E-mail: masaru.kato@ees.hokudai.ac.jp (MK); iyagi@ees.hokudai.ac.jp (IY)

Abstract

We prepared Sn-modified Pt(100), Pd(100) and Pd–Pt(100) single crystal electrodes and investigated the nitrate reduction reaction (NO_3RR) activity and the product selectivity for them using online electrochemical mass spectroscopy (OLEMS), also known as differential electrochemical mass spectroscopy (DEMS). OLEMS measurements allowed us to quantify volatile products of N_2, N_2O and NO and confirm the production of N_2 at Sn/Pd(100) but not at Sn/Pt(100). Pd-doping to Pt(100) with a 3 atomic % increased the product selectivity for the NO_3RR to N_2. These results indicate that the presence of Pd in the (100) surface is the key to produce N_2, which seems to be related to the hydrogen adsorption energy to the metal surface. The suppression of hydrogenation of intermediate species at the electrode surface could lead to the production of N_2. This work will guide us to understand N_2 production mechanism for the NO_3RR and develop highly selective electrocatalysts for denitrification.

Keywords

Nitrate reduction reaction; single crystal electrode; denitrification; differential electrochemical mass spectroscopy; online electrochemical mass spectroscopy

1. Introduction

Nitrate (NO_3^-) ions can be converted in natural biological processes including microbial denitrification to various inorganic compounds such as nitrite (NO_2^-) ions, nitric oxide (NO), nitrous oxide (N_2O), hydroxylammonium ions (NH_3OH^+), ammonium ions (NH_4^+) and dinitrogen (N_2). While many of these processes are essential to life, agricultural runoff and industrial waste streams can cause accumulation of excess NO_3^- and NO_2^- in groundwater, leading to negative impacts on global environments such as algal blooms, global warming and ozone layer depletion [1-3] and human health including methemoglobinemia (blue baby syndrome) and cancer [4,5]. To purify nitrate-contaminated groundwater or industrial water, electrocatalytic denitrification is a promising technology [5-8].

Electrocatalytic denitrification processes have advantages over thermocatalytic or biological processes because they require no additional chemical, can operate at ambient temperature and pressure, and can be powered by renewable energy [5-8]. Noble metal electrodes modified with p-block elements are known to show high electrocatalytic activity for the nitrate reduction reaction (NO_3RR). Sn is the most active promotor in the p-block elements for noble metal electrodes such as Pt [9-12] and Pd [10,12-14]. The surface modification of these noble metals with Sn accelerates the initial rate-determining step for the NO_3RR, NO_3^- to NO_2^-. Although Sn-modified Pt or Pd

electrodes have been widely studied for the electrocatalytic NO_3RR improvement, the exclusive production of the most environmentally friendly product dinitrogen (N_2) remains challenging.

Single crystal electrodes with low index surfaces provide us with a powerful platform to understand fundamental insights into the relationship of the surface structure with electrocatalytic activity and product selectivity. For the NO_3RR, Sn-modified Pt(100) electrodes tend to show higher electrocatalytic activity than Sn-modified Pt(111) electrodes [10]. For the NO_2^- reduction, the catalytic activity of single crystal platinum electrodes increases in the following order: Pt(111)<Pt(110)<<Pt(100) [5]. Density functional theory (DFT) calculations suggest that N–N bond formation can occur with lower barriers on the square lattice of the (100) surface as compared to the hexagonal (111) surface [15-17]. Furthermore, quasi-perfect Pt(100) surfaces are also unique in their sensitivity, achieving the direct conversion of NO_2^- to N_2 in alkaline solution [18,19]. These results encourage us to investigate the electrocatalytic activity and product selectivity of Sn-modified Pt(100) electrodes for the NO_3RR in acidic media. Compared with Pt electrodes, Pd electrodes are known to reduce NO to N_2 not only in alkaline media but also in acidic media [20]. Sn/Pd electrodes have a stronger tendency to the N–N bond formation than Sn/Rh, Sn/Pt and Sn/Ir [12], and Pd is one of the best (and few) catalysts for the N_2O reduction to N_2 with ~100% Faradaic

efficiency [21-23]. However, there is no report on the activity and selectivity of Sn-modified Pd(100) electrodes for the electrochemical NO_3RR.

Herein, we report the preparation of Sn-modified Pt(100), Pd(100) and Pd–Pt(100) electrodes and the analysis of gas species produced at them during the electrocatalytic NO_3RR in acidic media. To quantify the volatile products of NO, N_2O and N_2, an online electrochemical mass spectrometry (OLEMS), also known as differential electrochemical mass spectroscopy (DEMS), was used. The OLEMS is a powerful technique to detect volatile products produced at electrodes during electrochemical measurements [9,13,24]. The quantification of the volatile products allowed us to discuss the difference in the NO_3RR product selectivity between Pt(100) and Pd(100) and the effect of Pd-doping to Pt(100) on the product selectivity to N_2.

2. Experimental section

2.1. Materials

Perchloric acid (70%, purity: 99.999%; Sigma-Aldrich), sulfuric acid (99.999%, Sigma-Aldrich), tin(II) chloride dihydrate (97.0%, Kanto Chemical) and sodium nitrate (99.99%, Kanto Chemical) were purchased and used without further purification. Platinum wires (0.8 mmϕ or 0.5 mmϕ; 99.99% purity) and palladium (0.8 mmϕ or 0.5 mmϕ; 99.99% purity) wires were used for the preparation of single crystal electrodes.

Thin GORE PTFE membranes (VE91221, 0.32 mm in thickness) were provided by W. L. Gore & Associates. POREFLON membranes (HP-010-30; pore size: 0.1 μm; thickness: 30 μm) were provided by Sumitomo Electric Fine Polymer.

2.2. Preparation of single crystal electrodes

Pt, Pd and Pd–Pt alloy single crystal beads were prepared based on the procedure previously reported [10]. A platinum wire or a palladium wire was annealed in methane-oxygen flame to obtain a single crystal bead at the end of the wire. For the preparation of Pd–Pt alloy single crystal beads with 3 atomic % (at %) of Pd in Pt, a single crystal bead of Pt was used as a seed crystal as well as the source of Pt, and an amount of Pd was added to the Pt bead in methane-oxygen flame. The single crystal beads were oriented using the reflection of a He–Ne laser beam from a (100) facet on the single crystal bead, fixed in a poly(methyl methacrylate) resin (Technovit 4004, Heraeus Kulzer), cut in the direction of the (100) facet, and then polished with diamond slurries to be mirror-finished. The polished single crystal electrode was annealed in methane-oxygen flame at <1250 °C for 4 h. To confirm the preparation of the single crystal electrode with a specific orientation, cyclic voltammograms (CVs) were recorded in 0.5 M H_2SO_4 aqueous solution under Ar.

2.3. Electrochemical measurements

A glass-tubing chamber that has a gas inlet at the bottom and a gas outlet at the top was used for annealing electrodes. This chamber can keep Milli-Q water at the bottom. The Pt single crystal electrodes were annealed under H_2–Ar in the glass-tubing chamber that is placed in an induction coil of an induction heating system (EASY-HEAT model 0224, Ambrell), cooled under H_2–Ar, and then immersed in Milli-Q water purged with Ar in the same chamber. The surface of the electrode was covered with Milli-Q water and then transferred to the electrochemical cell for electrochemical measurements. Similarly, Pd and Pd–Pt alloy single crystal electrodes were annealed using the induction heating system. Pd–Pt electrodes were cooled and then immersed in Milli-Q water under H_2-Ar whereas Pd electrodes under Ar. The annealed electrode covered with a droplet of Milli-Q water was transferred to the electrochemical cell for electrochemical measurements. All electrochemical data were recorded on potentiostats (HZ7000, Hokuto Denko) equipped with a high-current booster (HZAP3003A, Hokuto Denko) using conventional three-electrode systems under Ar (99.999%, HOKKAIDO AIR WATER) with a Ag|AgCl (sat. KCl) electrode with a double junction holder (International chemistry) as the reference electrode and platinum foil coated with platinum black as the counter electrode. Single crystal electrodes were used as the working electrode. Electrolyte solutions were purged with Ar (99.999%) for at least 30 min before measurements. All electrochemical measurements were performed in the

hanging meniscus configuration. CVs on nitrate reduction were recorded in a 0.1 M $HClO_4$ aqueous solution containing 0.1 M $NaNO_3$ at a sweep rate of 10 mV s^{-1} under Ar. All potentials in the main text are shown against the reversible hydrogen electrode (RHE). The potentials against Ag|AgCl (sat. KCl) were converted to those against RHE using the following equation: *E* (*vs*. RHE) = *E* (*vs*. Ag|AgCl (sat. KCl)) +0.199 V + 0.059 V × pH.

The surface modification of single crystal electrodes with tin was carried out based on a reported procedure [10]. The annealed single crystal electrode covered with a droplet of Milli-Q water was immersed in 0.1 M $HClO_4$ aqueous solution containing 0.5 mM $SnCl_2$ for 30 s and then the electrode was immersed in Milli-Q water under Ar to remove excess tin species from the surface. The tin-modified electrode covered with a droplet of Milli-Q water was transferred to the electrochemical cell. CVs of tin-modified electrodes in the Hupd desorption region in 0.5 M H_2SO_4 aqueous solution allowed us to determine the tin surface coverage (θ_{Sn}) using the following equation: $\theta_{Sn} = (Q_H^0 - Q_H)/Q_H^0$, where Q_H^0 and Q_H indicate the Faradaic charges corresponding to the desorption of H_{upd} before and after the tin modification, respectively.

Auger electron spectroscopy

Auger electron spectra were recorded in a derivative mode on JAMP-9500F (JEOL) using the 10 keV electron beam energy, 1 eV modulation, and 10 nA beam current in the range from 30 to 2500 eV.

Online electrochemical mass spectrometry (OLEMS) system.

An OLEMS setup was constructed according to the literature [25]. The OLEMS setup consists of a quadrupole mass spectrometer (M201QA-TDM, CANON ANELVA), metal ionization gauge (GI-M2, ULVAC), a rotary vane vacuum pump (GLD-135, ULVAC) and a turbo molecular vacuum pump (5150 Turbo Pump, Alcatel) equipped with a controller (CFF450, Alcatel). A glass pinhole was used as the gas inlet to the mass spectrometer. This pinhole was covered with a thin GORE PTFE membrane (VE91221, 0.32 mm in thickness) and a POREFLON membrane (HP-010-30; pore size: 0.1 μm; thickness: 30 μm) and then heated with a heat gun. The inner diameter of the pinhole was below 10 μm. The working electrode was set in the hanging meniscus configuration and the pinhole was placed underneath the electrode surface within 30 μm. The internal pressure was $3–4\times10^{-4}$ Pa during the OLEMS experiments.

Product analysis for electrocatalytic nitrate reduction.

The single crystal electrode used was annealed in the same procedure for standard electrochemical measurements. To confirm the clean surface of the electrode, CVs were recorded in 0.5 M degassed H_2SO_4 aq. Sweep rates were 50 mV s^{-1} for Pt and Pd–Pt

alloy electrodes and 20 mV s^{-1} for Pd electrodes. After the electrochemical measurements in 0.5 M H_2SO_4 aq. under Ar, the electrode covered with a droplet of 0.5 M H_2SO_4 aq. was transferred to a degassed 0.1 M $HClO_4$ aqueous solution containing 0.5 mM $SnCl_2$ and then kept in the solution for 30 s. The electrode covered with a droplet of the $SnCl_2$ solution was to a degassed Milli-Q water and then cleaned in it. The electrode covered with Milli-Q water was transferred again to 0.5 M degassed H_2SO_4 aq. to record CVs again and confirm the surface modification with Sn species. Note that all solutions used in the above processes were degassed with Ar for at least 30 min.

For OLEMS, an electrolyte aqueous solution containing 0.1 M $HClO_4$ and 0.1 M $NaNO_3$ was used. This solution was purged with Ar for at least 30 min before use. The tin-modified electrode covered with a drop of 0.5 M degassed H_2SO_4 aq. was transferred to a degassed Milli-Q water and then cleaned in it. The electrode covered with a drop of Milli-Q water was transferred to the 0.1 M $HClO_4$ solution containing $NaNO_3$ under Ar. CVs were recorded at a sweep rate of 1 mV s^{-1} from +0.40 to –0.05 V and then +0.40 V vs. RHE under Ar.

Although quantitative analysis of OLEMS data remains challenging, we roughly quantified amounts of gasous products for the NO_3RR, and then calculated Faradaic

efficiencies of the production of them. The details are described in the Supplimentary Data.

3. Results and discussion

3.1 Characterization of Pt(100), Pd(100) and Pd–Pt(100).

To confirm the preparation of Pt(100) electrodes, CVs of Pt(100) were recorded in a 0.5 M H_2SO_4 aqueous solution under Ar (**Fig. 1a**). The symmetric CV indicates that the electrochemical processes on the surface were reversible [26]. Characteristic waves in the potential range between +0.2 and +0.45 V vs. RHE are associated with adsorption and desorption of underpotentially deposited hydrogen, H_{upd} [27]. The sharp peak at +0.37 V vs. RHE is associated with extended (1x1)–Pt(100) long-range order [28]. The peak at +0.27 V vs. RHE was assigned to defect sites at the edge of (100) terraces [29]. These electrochemical features allowed us to confirm the successful preparation of Pt(100) electrodes.

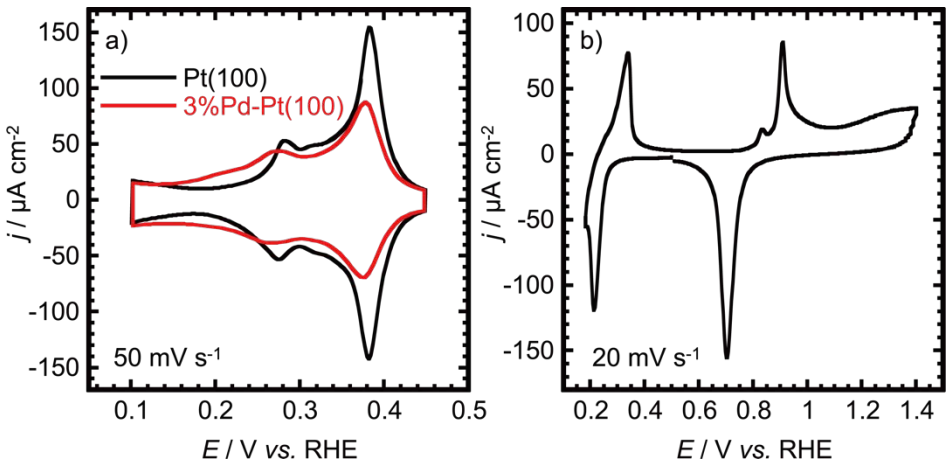

Fig. 1 Representative CVs of (a) Pt(100) (the trace in black) and 3 at % Pd–Pt(100) (the trace in red) and (b) Pd(100). CVs were recorded at a sweep rate of 50 mV s^{-1} for Pt(100) and Pd–Pt(100) and 20 mV s^{-1} for Pd(100) in a 0.5 M H_2SO_4 aqueous solution under Ar.

CVs of Pd(100) were also recorded in a 0.5 M H_2SO_4 aqueous solution under Ar (**Fig. 1b**). A sharp anodic peak at ca. +0.35 V vs. RHE and a sharp cathodic peak at ca. +0.22 V were observed and associated with desorption and adsorption of sulfate anions, respectively [30,31]. At ≤ ca. +0.3 V vs. RHE, cathodic currents involving hydrogen absorption into palladium bulk are known to overlap with the adsorption of sulfate anions. We also observed anodic and cathodic peaks at ca. +0.90 and +0.73 V vs. RHE, respectively. These are assigned to be the formation of the surface oxide and reduction of it, respectively. The peak potential of the Pd surface oxide formation is sensitive to the surface structure: the higher the surface atomic density is, the more positive the peak position of the oxide formation is [30,32]. The peak potential observed was in good agreement with Pd(100) single crystal electrodes previously reported [30], allowing us to confirm the preparation of Pd(100) electrodes.

We prepared Pd-Pt(100) electrodes with a 3 at % of Pd in Pt. Pd was added into a Pt bead as the seed crystal in methane–oxygen flame to prepare a Pd–Pt alloy single crystal bead because the melting point of Pt (2041 K) is higher than that of Pd (1828 K) and the melting seed crystal must retain to obtain a uniform alloy *via* the convection of the molten metal [33]. A representative CV of the prepared Pd–Pt(100) electrode was

shown in **Fig. 1a**. Although the Pd–Pt(100) showed a similar redox behavior to Pt(100), the peak intensity at ca. +0.37 V decreases, and the peak position shifts to more negative potentials, compared with the CV of Pt(100). Furthermore, such negative peak shifts were also observed for hydrogen adsorption/desorption peaks at (100) terrace edges at ca. +0.27 V. These results indicate that the Pd–Pt alloy formation weakens the Pt–H bonding for the H_{upd} at the surface. Similar changes were already reported for Pd–Pt(100) alloy electrodes with different bulk compositions [28,34]. An Auger electron spectrum of Pd–Pt(100) (**Fig. S1**) indicated that the pure Pt(100) was replaced by surface alloy phases for Pd–Pt(100) alloys. This spectrum also enabled us to determine an atomic percentage of Pd at the surface to be ca. 12 at %, which was greater than 3at % in the bulk. For previously prepared Pd–Pt(100) single crystal electrodes, the amount of palladium at the surface for Pd–Pt(100) was also greater than that in the bulk [28]. Thus, it is most likely that the amount of palladium at the surface of Pd–Pt(100) that we prepared is also greater than that in the bulk.

3.2 Electrocatalytic NO_3RR at Sn/Pt(100), Sn/Pd(100) and Sn/Pd–Pt(100) electrodes.

CVs of tin-modified and unmodified Pd(100) electrodes were recorded in the presence of nitrate under Ar to understand the electrocatalytic NO_3RR activity (**Fig.**

2b). This is the first report on the electrocatalytic NO_3RR for Sn/Pd(100) electrodes and therefore we collected CVs particularly for tin-modified Pd(100) electrodes with different surface coverages of tin (θ_{Sn}). The surface of Pd(100) electrodes was modified with tin species, which are possibly composed of metallic Sn and $Sn^{II}(OH)_x$ species [10,11], and then tin surface coverages (θ_{Sn}) were determined based on the hydrogen desorption peak (**Fig. S2**) [10]. With low θ_{Sn} values, Pd(100) showed almost no catalytic currents whereas cathodic currents involving NO_3RR were observed for the Pd(100) electrodes with θ_{Sn} = 0.71 and 0.91 (**Fig. S3**). This activity dependence on θ_{Sn} is similar to those previously reported tin-modified palladium electrodes [14]. The Sn/Pd(100) electrodes with θ_{Sn} = 0.71 and 0.91 showed almost the same catalytic current densities of ca. –16 mA cm^{-2} at 0.01 V vs. RHE. In the negative-going sweep, cathodic currents increased and maximized at ca. 0.13 V vs. RHE but decreased at < 0.13 V vs. RHE for Sn/Pd(100) electrodes with θ_{Sn} = 0.71 and 0.91. Similar deactivation processes were also observed at potentials lower than 0.12 V for tin-modified platinum electrodes including Sn/Pt(poly) [9,35], Sn/Pt(111) and Sn/Pd–Pt(111) with low $\theta_{Sn} \leq 0.4$ [10]. The deactivation of these electrodes is associated with the formation of strongly adsorbed hydrogen on platinum [9]. Interestingly, the deactivation for Sn/Pd(100) was observed even with high θ_{Sn} of 0.71 and 0.91 (**Figs. 2b** and **S3**), indicating that specific adsorption processes of other species could be

involved: for example, nitric oxide is known to adsorb on metal surfaces including platinum [36,37]. Because no such deactivation was observed for Sn/Pt(100) and Sn/Pd-Pt(100) electrodes, the nitrate reduction activity on Sn/Pd(100) is highly sensitive to the specific adsorption of products.

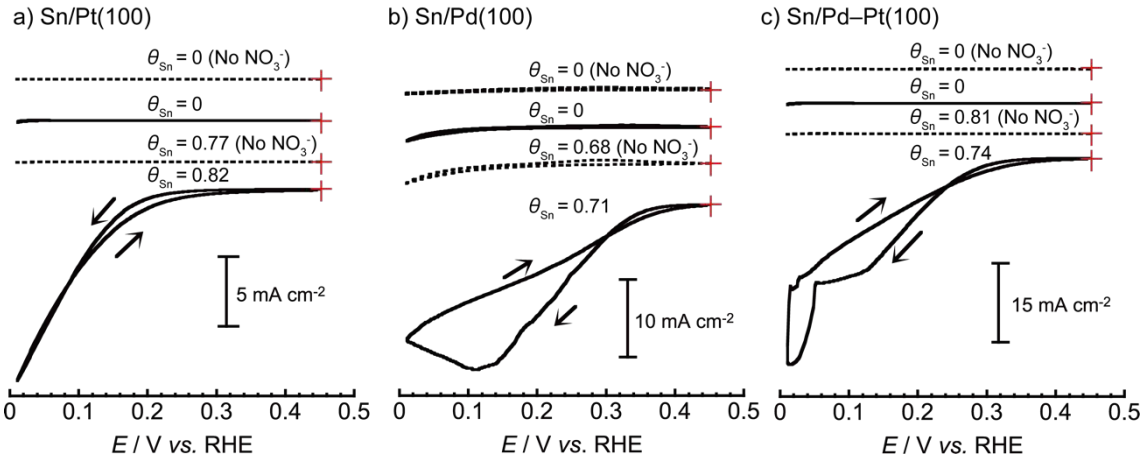

Fig. 2 CVs of (a) Sn/Pt(100), (b) Sn/Pd(100) and (c) Sn/Pd–Pt(100) recorded at 10 mV s^{-1} in a 0.1 M $HClO_4$ aqueous solution in the presence (the solid lines) and the absence (the broken lines) of 0.1 M $NaNO_3$ under Ar. Arrows in black and plus signs in red indicate the sweep direction and the initial position of the CV, respectively.

We also prepared Sn/Pt(100) and Sn/Pd–Pt(100) electrodes based on the preparation procedure previously reported [10]. Although unmodified Pt(100) and Pd–Pt(100) electrodes are known to show the NO_3RR activity [38], their activities were much lower than those of tin-modified electrodes (**Figs. 2a and 2c**). Thus, the tin-modification gave a drastic increase of the NO_3RR activity to Pt(100) and Pd–Pt(100) electrodes. Since a tin coverage range between 0.7 to 0.8 maximized the electrocatalytic NO_3RR activity

for tin-modified (100) electrodes we prepared in this work, we used Sn/Pt(100) and Sn/Pd-Pt(100) electrodes with θ_{Sn}~0.75 for the further studies.

3.3 Product analysis of electrocatalytic NO_3RR using OLEMS.

To analyze products for the electrochemical NO_3RR produced at single crystal electrodes, an online electrochemical mass spectroscopy (OLEMS) setup, also known as differential electrochemical mass spectroscopy (DEMS), was constructed as shown in **Fig. 3** [25]. In our setup, the glass pinhole, which was covered with porous PTFE membranes, was placed close to the surface of the working electrode and used as the gas inlet to the mass spectrometer to analyze gaseous products (**Fig. 3b**).

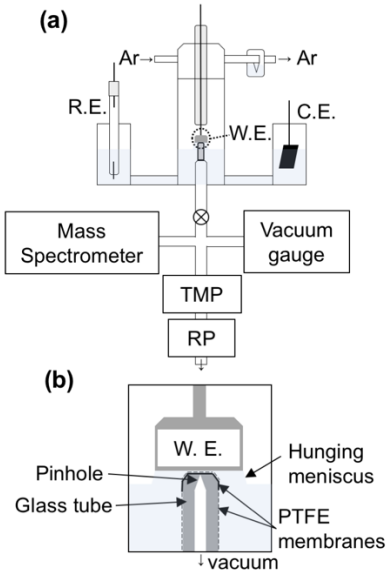

Fig. 3. The OLEMS setup used in this work.

LSVs and OLEMS results allowed us to understand the potential dependence of volatile products of NO, N_2O and N_2 for Sn/Pt(100), Sn/Pd(100) and Sn/Pd–Pt(100)

electrodes (**Fig. 4**). All electrodes showed cathodic currents for the NO_3RR at <0.3 V vs. RHE (**Fig. 4a**) and associated mass signals for the volatile products also increased at <0.3 V vs. RHE (**Fig. 4b–c**). Although quantitative analysis of OLEMS data remains challenging, we approximately quantified amounts of volatile products and then calculated Faradaic efficiencies of them (See more details in the Supplementary data). Our calculation indicates that the Sn/Pt(100) electrode produced volatile products of NO and N_2O with a Faradaic efficiency of ca. 25% (**Fig. S6a**), indicating that non-volatile products of NH_3 and NH_2OH, which was reported as the main product for tin-modified platinum polycrystalline electrodes [39], were mainly produced at Sn/Pt(100) rather than the volatile products. It is most likely that H_{upd} atoms on the Pt surface are involved in the production of non-volatile products [11,40,41].

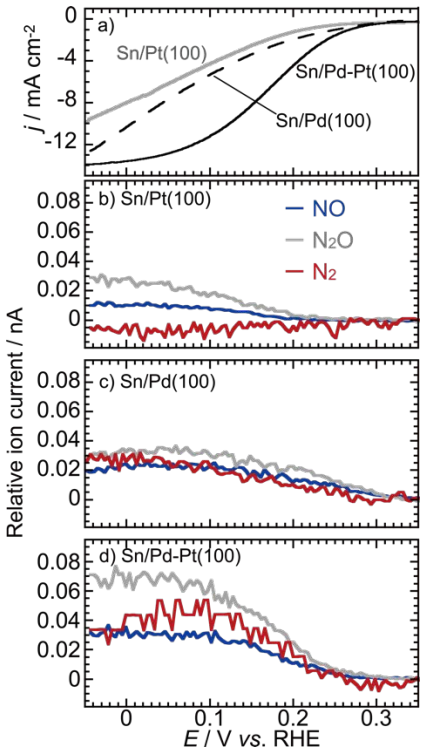

Fig. 4 (a) Linear sweep voltammograms recorded in the negative-going sweep at 1 mV s^{-1} in a 0.1 M $HClO_4$ aqueous solution containing 0.1 M $NaNO_3$ under Ar and the associated mass signals of NO (the traces in blue), N_2O (the traces in gray) and N_2 (the traces in red) for (b) Sn/Pt(100), (c) Sn/Pd(100) and (d) Sn/Pd–Pt(100). The tin coverages of θ_{Sn} for Sn/Pt(100), Sn/Pd(100) and Sn/Pd–Pt(100) were 0.80, 0.71 and 0.82, respectively.

In contrast to Sn/Pt(100), Sn/Pd(100) produced not only NO and N_2O but also N_2 (**Fig. 4c**). A Faradaic efficiency for the production of these gases reached ca. 92% at +0.2 V vs. RHE and N_2 accounted for 34% (**Fig. S6b**). At polycrystalline palladium electrodes, N_2 was produced for the electrochemical nitric oxide reduction in acidic media but not at polycrystalline platinum electrodes [20]. Thus, the efficient reduction of NO to N_2 proceeds at the Pd(100) surface rather than the production of non-volatile products. Interestingly, Faradaic efficiencies of the total gaseous products dropped from 92% at 0.2 V vs. RHE to ca. 50% at ≤ 0.15 V vs. RHE for Sn/Pd(100) (**Fig. S6b**) but still higher than those obtained for Sn/Pt(100) (**Fig. S6a**). The formation of non-volatile products such as NH_2OH [13] could be suppressed at Sn/Pd(100), compared with Sn/Pt(100), even in the H_{upd} potential range (**Fig. 1b**).

The 3% doping of Pd into Pt(100) gave a huge impact on the product distribution and produced N_2 (**Fig. 4d**), which was not detected for Sn/Pt(100) (**Fig. 4b**). Sn/Pd–Pt(100) produced the volatile products with a Faradaic efficiency of ca. 60% in the potential range between 0.1 and 0.2 V vs. RHE (**Fig. S6c**). Compared with Sn/Pt(100),

the Sn/Pd–Pt(100) electrode suppressed the formation of non-volatile products such as NH_2OH or consecutively converted them to N_2.

For the formation of N_2 for the NO_3RR at Pt and Pd electrodes, four reaction pathways have been proposed [4-7,9]:

$$N_2O + 2H^+ + 2e^- \rightarrow N_2 + 2H_2O \quad (1)$$

$$HNO_{(ad)} + NH_2OH \rightarrow N_2 + 2H_2O \quad (2)$$

$$NH_{2(ad)} + NO_{(ad)} \rightarrow N_2 + H_2O \quad (3)$$

$$2N_{(ad)} \rightarrow N_2 \quad (4)$$

N_2O can be reduced to N_2 at Sn/Pd–Pt(100) following Reaction (1). N_2O can be formed *via* an electrocatalytic dimerization between $NO_{(ad)}$ at the surface and $NO_{(aq)}$ in solution in an Eley-Rideal-like mechanism [20] rather than the Langmuir-Hinshelwood-like mechanism between two $NO_{(ad)}$ species [42]. Reaction (1) can be responsible for N_2 production during the nitrate reduction even at Sn-modified Pt electrodes particularly in long-term electrolysis experiments, where it proceeds at the remaining free Pt sites [9,35]. Since Pd efficiently drives the electrocatalytic N_2O reduction to N_2 [21,22], Reaction (1) can be accelerated at Sn/Pd–Pt(100), compared with Sn/Pt(100). N_2O has moderate solubility in water (~24 mmol L^{-1}) [3,43] and solubilized N_2O can be susceptible to be reduced after re-adsorption [7,44].

Another plausible reaction pathway at Sn/Pd–Pt(100) is Reaction (2): NO adsorbed on the electrode surface ($NO_{(ad)}$) can be converted to NH_2OH *via* $HNO_{(ad)}$, where NH_2OH could react with $HNO_{(ad)}$ to produce N_2 and H_2O [6,7,43]. This reaction pathway was proposed as one of the plausible pathways for a tin cathode [43]. Although there is no experimental confirmation of the production of NH_2OH in this work, NH_2OH can be produced at Sn/Pt(100) because tin-modified polycrystalline platinum electrodes are known to produce NH_2OH as the main product in the non-volatile products [39]. Reaction (2) occurs even in acidic media, where NH_2OH should be hydroxylammonium (NH_3OH^+) [9].

Reaction (3) is unlikely in acidic media although it is proposed for Pt(100) in alkaline media [5,18,19]. Reaction (3) follows a Langmuir-Hinshelwood recombination reaction between $NO_{(ad)}$ and $NH_{2(ad)}$ *via* a transient species of N-nitrosamide ($NONH_2$) [5,7,18,19] and is sensitive to solution pH: the electrocatalytic activity of Pt(100) drops as the pH decreases and approaches the pK_a of NH_4^+ (pK_a = 9.3 for NH_4^+) [19]. DFT calculations also suggest that metals with stronger adsorption of $H_{(ad)}$ have lower activation energy for hydrogenation reactions involving $N_{(ad)}$, $NH_{(ad)}$ and $NH_{2(ad)}$ [45]. This means that metal surfaces with weaker $H_{(ad)}$ adsorption tend to show higher activation energy for the hydrogenation reactions. Since Pd–Pt(100) has weaker hydrogen adsorption than Pt(100) (**Fig. 1a**), the formation of $NH_{2(ad)}$ in Reaction (3) can

be expected to be more suppressed at Sn/Pd–Pt(100) than at Pt(100), which allowed us to exclude Reaction (3) as the main reaction pathway for Sn/Pd–Pt(100). Regarding Reaction (4), this mechanism has not been confirmed experimentally yet [7,43] and the contribution of it remains unclear although this reaction is considered as an elementary step to N_2 in DFT calculations [15,45].

4. Conclusions

Pt(100), Pd(100) and Pd–Pt(100) with 3 at % of Pd electrodes were prepared. Although these electrodes showed almost no activity for the NO_3RR in acidic media, the surface modification with tin activated them for the NO_3RR. The quantification of volatile products allowed us to confirm that Sn/Pd(100) and Sn/Pd–Pt(100) produced N_2 but Sn/Pt(100) did not. These results indicate that Sn and Pd serve as the promotor for the initial rate-determining step of the NO_3RR, NO_3^- to NO_2^-, and the selector to N_2, respectively. Since Pd–Pt(100) exhibited a weaker affinity with hydrogen adatoms than Pt(100), tuning of hydrogen adsorption energy for metal alloys would be a key to the selective production of dinitrogen. NO is produced as a key intermediate species to the N_2 formation and it is highly likely that the NO binding to the electrode surface can be affected by the tin modification: surface availability and NO binding ability. To understand the main reaction pathway for the NO_3RR to N_2 at Sn/Pd(100) or Sn/Pd–

Pt(100), further electrochemical and spectroscopic studies on not only the NO_3RR but also the NO reduction reaction using spectroscopic techniques such as *in situ* FTIR spectroscopy [36,37,46] are needed.

Acknowledgments

The authors thank Takao Ohta (Graduate School of Engineering, Hokkaido University) and Katsuhisa Ishikawa, Takahiko Hasegawa (Technical Division, Institute for Catalysis, Hokkaido University) for their technical support on electrochemical glassware, and Dr. Kazuhide Kamiya (Osaka University) and Dr. Jun Hirokawa (Hokkaido University) for their fruitful discussion on the OLEMS setup. Auger electron scopy was conducted at Laboratory of XPS analysis, Joint-use facilities, Hokkaido University. This work was partially supported by Grant-in-Aid for Young Scientists (B) (No. 16K20882 to MK), Scientific Research (B) (No. 19H02664 to I.Y.), and the project “Development of Advanced PEFC Utilization Technologies/Development of Fundamental Technologies for PEFC Promotion/Highly-Coupled Analysis of Phenomena in MEA and its Constituents and Evaluation of Cell Performance” of NEDO, Japan.

References

[1] A.R. Ravishankara, J.S. Daniel, R.W. Portmann, Science, **326**, 123-125 (2009).
https://doi.org/10.1126/science.1176985

[2] H. Tian, R. Xu, J.G. Canadell, R.L. Thompson, W. Winiwarter, P. Suntharalingam, E.A. Davidson, P. Ciais, R.B. Jackson, G. Janssens-Maenhout, M.J. Prather, P. Regnier, N. Pan, S. Pan, G.P. Peters, H. Shi, F.N. Tubiello, S. Zaehle, F. Zhou, A. Arneth, G. Battaglia, S. Berthet, L. Bopp, A.F. Bouwman, E.T. Buitenhuis, J. Chang, M.P. Chipperfield, S.R.S. Dangal, E. Dlugokencky, J.W. Elkins, B.D. Eyre, B. Fu, B. Hall, A. Ito, F. Joos, P.B. Krummel, A. Landolfi, G.G. Laruelle, R. Lauerwald, W. Li, S. Lienert, T. Maavara, M. MacLeod, D.B. Millet, S. Olin, P.K. Patra, R.G. Prinn, P.A. Raymond, D.J. Ruiz, G.R. van der Werf, N. Vuichard, J. Wang, R.F. Weiss, K.C. Wells, C. Wilson, J. Yang, Y. Yao, Nature, **586**, 248-256 (2020).
https://doi.org/10.1038/s41586-020-2780-0

[3] W.C. Trogler, Coord. Chem. Rev., **187**, 303-327 (1999).
https://doi.org/10.1016/S0010-8545(98)00254-9

[4] K.A. Karanasios, I.A. Vasiliadou, S. Pavlou, D.V. Vayenas, J. Hazard. Mater., **180**, 20-37 (2010).
https://doi.org/10.1016/j.jhazmat.2010.04.090

[5] M. Duca, M.T.M. Koper, Energy Environ. Sci., **5**, 9726-9742 (2012).
https://doi.org/10.1039/C2EE23062C

[6] Y. Zeng, C. Priest, G. Wang, G. Wu, Small Methods, **4**, 2000672 (2020).
https://doi.org/10.1002/smtd.202000672

[7] S. Garcia-Segura, M. Lanzarini-Lopes, K. Hristovski, P. Westerhoff, Appl. Catal. B: Environ., **236**, 546-568 (2018).
https://doi.org/10.1016/j.apcatb.2018.05.041

[8] N. Singh, B.R. Goldsmith, ACS Catal., **10**, 3365-3371 (2020).
https://doi.org/10.1021/acscatal.9b04167

[9] J. Yang, M. Duca, K.J.P. Schouten, M.T.M. Koper, J. Electroanal. Chem., **662**, 87-92 (2011).
https://doi.org/10.1016/j.jelechem.2011.03.015

[10] M. Kato, M. Okui, S. Taguchi, I. Yagi, J. Electroanal. Chem., **800**, 46-53 (2017).
https://doi.org/10.1016/j.jelechem.2017.01.020

[11] J. Yang, F. Calle-Vallejo, M. Duca, M.T.M. Koper, ChemCatChem, **5**, 1773-1783 (2013).
https://doi.org/10.1002/cctc.201300075

[12] S. Piao, Y. Kayama, Y. Nakano, K. Nakata, Y. Yoshinaga, K. Shimazu, J. Electroanal. Chem., **629**, 110-116 (2009).
https://doi.org/10.1016/j.jelechem.2009.01.031

[13] Y.Y. Birdja, J. Yang, M.T.M. Koper, Electrochim. Acta, **140**, 518-524 (2014).
https://doi.org/10.1016/j.electacta.2014.06.011

[14] K. Shimazu, R. Goto, S. Piao, R. Kayama, K. Nakata, Y. Yoshinaga, J. Electroanal. Chem., **601**, 161-168 (2007).

https://doi.org/10.1016/j.jelechem.2006.11.005
[15] H.-J. Chun, V. Apaja, A. Clayborne, K. Honkala, J. Greeley, ACS Catal., **7**, 3869-3882 (2017).
https://doi.org/10.1021/acscatal.7b00547
[16] D. Skachkov, C. Venkateswara Rao, Y. Ishikawa, J. Phys. Chem. C, **117**, 25451-25466 (2013).
https://doi.org/10.1021/jp4048874
[17] H. Li, Y. Li, M.T.M. Koper, F. Calle-Vallejo, J. Am. Chem. Soc., **136**, 15694-15701 (2014).
https://doi.org/10.1021/ja508649p
[18] M. Duca, M.C. Figueiredo, V. Climent, P. Rodriguez, J.M. Feliu, M.T.M. Koper, J. Am. Chem. Soc., **133**, 10928-10939 (2011).
https://doi.org/10.1021/ja203234v
[19] M. Duca, M.O. Cucarella, P. Rodriguez, M.T.M. Koper, J. Am. Chem. Soc., **132**, 18042-18044 (2010).
https://doi.org/10.1021/ja1092503
[20] A.C.A. de Vooys, M.T.M. Koper, R.A. van Santen, J.A.R. van Veen, J. Catal., **202**, 387-394 (2001).
https://doi.org/10.1006/jcat.2001.3275
[21] B. Wang, X.-y. Li, Anal. Chem., **70**, 2181-2187 (1998).
https://doi.org/10.1021/ac970601h
[22] A. Kudo, A. Mine, J. Electroanal. Chem., **408**, 267-269 (1996).
https://doi.org/10.1016/0022-0728(96)04630-X
[23] K.H. Kim, T. Lim, M.J. Kim, S. Choe, S. Baek, J.J. Kim, Electrochem. Commun., **62**, 13-16 (2016).
https://doi.org/10.1016/j.elecom.2015.11.002
[24] N. Todoroki, H. Tsurumaki, H. Tei, T. Mochizuki, T. Wadayama, J. Electrochem. Soc., **167**, 106503 (2020).
https://doi.org/10.1149/1945-7111/ab9960
[25] Y. Qu, L. Wang, C. Li, Y. Gao, J. Kyong Sik, J. Rao, G. Yin, Int. J. Hydrog. Energy, **42**, 228-235 (2017).
https://doi.org/10.1016/j.ijhydene.2016.08.215
[26] A. Zolfaghari, G. Jerkiewicz, J. Electroanal. Chem., **420**, 11-15 (1997).
https://doi.org/10.1016/S0022-0728(96)01020-0
[27] J. Clavilier, J.M. Feliu, A. Fernandez-Vega, A. Aldaz, J. Electroanal. Chem. Interf. Electrochem., **269**, 175-189 (1989).
https://doi.org/10.1016/0022-0728(89)80111-1
[28] D.J. Watson, G.A. Attard, Surf. Sci., **515**, 87-93 (2002).
https://doi.org/10.1016/S0039-6028(02)01811-3
[29] S. Motoo, N. Furuya, Berichte der Bunsengesellschaft für physikalische Chemie, **91**, 457-461 (1987).
https://doi.org/10.1002/bbpc.19870910446
[30] N. Hoshi, K. Kagaya, Y. Hori, J. Electroanal. Chem., **485**, 55-60 (2000).
https://doi.org/10.1016/S0022-0728(00)00098-X

[31] N. Hoshi, M. Kuroda, O. Koga, Y. Hori, J. Phys. Chem. B, **106**, 9107-9113 (2002).
https://doi.org/10.1021/jp020898+
[32] K. Sashikata, Y. Matsui, K. Itaya, M.P. Soriaga, J. Phys. Chem., **100**, 20027-20034 (1996).
https://doi.org/10.1021/jp9620532
[33] M. Wakisaka, Y. Hyuga, K. Abe, H. Uchida, M. Watanabe, Electrochem. Commun., **13**, 317-320 (2011).
https://doi.org/10.1016/j.elecom.2011.01.013
[34] F.J. Vidal-Iglesias, A. Al-Akl, D. Watson, G.A. Attard, J. Electroanal. Chem., **611**, 117-125 (2007).
https://doi.org/10.1016/j.jelechem.2007.08.005
[35] K. Tada, K. Shimazu, J. Electroanal. Chem., **577**, 303-309 (2005).
https://doi.org/10.1016/j.jelechem.2004.11.039
[36] B. Álvarez, A. Rodes, J.M. Pérez, J.M. Feliu, J.L. Rodríguez, E. Pastor, Langmuir, **16**, 4695-4705 (2000).
https://doi.org/10.1021/la991473q
[37] I. Katsounaros, M.C. Figueiredo, X. Chen, F. Calle-Vallejo, M.T.M. Koper, ACS Catal., **7**, 4660-4667 (2017).
https://doi.org/10.1021/acscatal.7b01069
[38] I. Katsounaros, M.C. Figueiredo, X. Chen, F. Calle-Vallejo, M.T.M. Koper, Electrochim. Acta, **271**, 77-83 (2018).
https://doi.org/https://doi.org/10.1016/j.electacta.2018.03.126
[39] J. Yang, Y. Kwon, M. Duca, M.T.M. Koper, Anal. Chem., **85**, 7645-7649 (2013).
https://doi.org/10.1021/ac401571w
[40] K. Nishimura, K. Machida, M. Enyo, Electrochim. Acta, **36**, 877-880 (1991).
https://doi.org/10.1016/0013-4686(91)85288-I
[41] G.E. Dima, A.C.A. de Vooys, M.T.M. Koper, J. Electroanal. Chem., **554-555**, 15-23 (2003).
https://doi.org/10.1016/S0022-0728(02)01443-2
[42] A. Clayborne, H.-J. Chun, R.B. Rankin, J. Greeley, Angew. Chem. Int. Ed., **54**, 8255-8258 (2015).
https://doi.org/10.1002/anie.201502104
[43] I. Katsounaros, G. Kyriacou, Electrochim. Acta, **53**, 5477-5484 (2008).
https://doi.org/10.1016/j.electacta.2008.03.018
[44] M.T. de Groot, M.T.M. Koper, J. Electroanal. Chem., **562**, 81-94 (2004).
https://doi.org/10.1016/j.jelechem.2003.08.011
[45] J.-X. Liu, D. Richards, N. Singh, B.R. Goldsmith, ACS Catal., **9**, 7052-7064 (2019).
https://doi.org/10.1021/acscatal.9b02179
[46] J. Souza-Garcia, E.A. Ticianelli, V. Climent, J.M. Feliu, Electrochim. Acta, **54**, 2094-2101 (2009).
https://doi.org/10.1016/j.electacta.2008.08.059

Graphical abstract

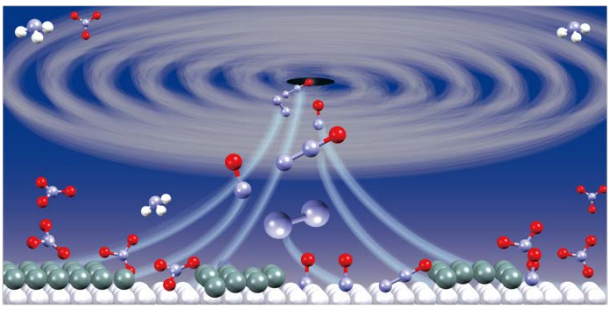

Highlights

- Sn/Pt(100), Sn/Pd(100) and Sn/Pd–Pt(100) were prepared for the nitrate reduction.

- Gasous products for the electrochemical NO_3RR were analyzed using OLEMS.

- Sn/Pd(100) and Sn/Pd-Pt(100) produced N_2 but not Sn/Pt(100).